Technical Note	LIGO-T080144-00-I	2008/10/30

The Enhanced LIGO Output Mode Cleaners

S J Waldman

California Institute of Technology
LIGO Project, MS 18-34
Pasadena, CA 91125
Phone (626) 395-2129
Fax (626) 304-9834
E-mail: info@ligo.caltech.edu

Massachusetts Institute of Technology
LIGO Project, Room NW22-295
Cambridge, MA 02139
Phone (617) 253-4824
Fax (617) 253-7014
E-mail: info@ligo.mit.edu

LIGO Hanford Observatory
Route 10, Mile Marker 2
Richland, WA 99352
Phone (509) 372-8106
Fax (509) 372-8137
E-mail: info@ligo.caltech.edu

LIGO Livingston Observatory
19100 LIGO Lane
Livingston, LA 70754
Phone (225) 686-3100
Fax (225) 686-7189
E-mail: info@ligo.caltech.edu

http://www.ligo.caltech.edu/

Abstract

This note describes the Enhanced LIGO output mode cleaner design and construction. Included are the choice of photodiodes, breadboard dimensions and mass, cavity g-factor and finesse. The appendix collects the as-built data for both the L1 and H1 output mode cleaners.

1 DC readout requirements

DC readout represents a significant shift in paradigm for the readout of the LIGO Differential Arm length degree of freedom (DARM). Historically, all of the lengths in the LIGO interferometer have been read out using heterodyne detection in which a pair of auxiliary optical sideband fields beat against the carrier field to generate a Pound-Drever-Hall error signal [**?**]. This technique provides a linear error signal with excellent shot-noise limited sensitivity that can be used to control the interferometer (IFO) lengths. Unfortunately, the RF sideband fields are relatively noisy compared to the carrier field because the sidebands don't resonate in the arm cavities and hence aren't filter by the $\sim 1\ Hz$ coupled-cavity pole. Compounding the problem, the sidebands resonate in the recycling cavity which is nearly unstable (g factor ~ 1) so that the RF sideband spatial mode fluctuates relative to the carrier.

1.1 Basic theory

DC readout sidesteps many of the problems with RF readout by using the carrier field itself as a reference to generate an error signal. On resonance, the carrier light from each arm interferes at the beam splitter such that the anti-symmetric port (AS port) is (ideally) perfectly dark. With the other lengths held constant, a DARM shift generates an an equal and opposite phase shift in carrier light from each arm such that the AS port is no longer dark. For a DARM length change x, a simple cavity calculation shows that the power at the AS port scales as

$$P_{DC}(x) = 4\ r_2^2\ g_{cav}^2 P_{BS} \frac{\sin^2[kx]\ \cos^2[kx]}{1 + 4(F/\pi)^2 \sin^2[kx]} \tag{1}$$

$$\simeq 4\ r_2^2\ g_{cav}^2\ P_{BS}\ (kx)^2. \tag{2}$$

Here $r_2 = \sqrt{1 - t_2^2}$ is the amplitude reflectivity of the Fabry-Perot arm cavity end mirrors, t_2 is the amplitude transmissivity, P_{BS} is the power incident on the beamsplitter (from the power recycling mirror), and $k = 2\pi/\lambda$ is the wavenumber. The input mirror reflectivity (transmissivity) is r_1 (t_1). The arm cavity gain, $g_{cav} = t_1^2/(1 - r_1 r_2)^2$, is the ratio of the power circulating in the cavity to the power incident on the input coupler on resonance. The arm cavity finesse, $F = \pi\sqrt{r_1 r_2}/(1 - r_1 r_2)$, is the ratio of the full-width, half-max of a fringe to the spacing between fringes. For LIGO, $\lambda = 1.064\ \mu m$, $g \approx 138$, and $F \approx 226$. Since the end mirrors of the LIGO arm cavities are essentially perfect reflectors ($T_2 \approx 6\ ppm$) we set $r_2^2 = 1$ in the following.
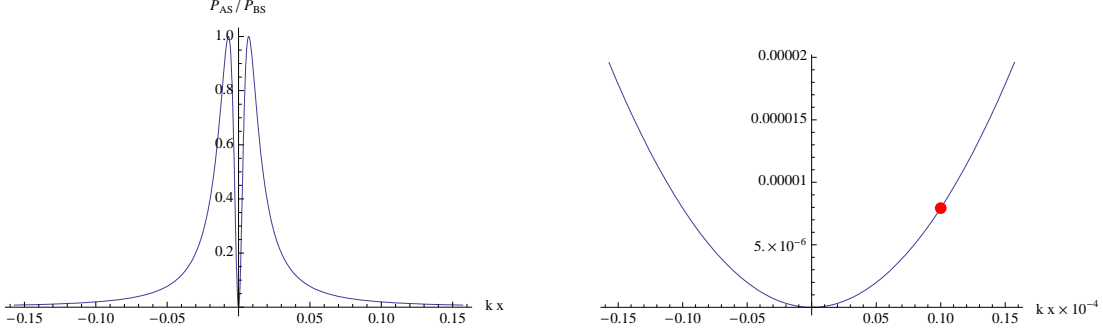
Figure 1: A Fabry-Perot Michelson fringe as seen from the AS port.

The readout method is illustrated in Fig. 1 which shows the DARM fringe at the AS port. Note that the left hand figure shows a span of $kx = \pm\pi/20$ while the right hand panel is zoomed in by a factor of 10^4. For such small displacements, the fringe is quadratic and well approximated by the expansion in Eq. 1. In order to recover a linear sensitivity to the DARM offset, the IFO is intentionally offset from the fringe by, for example, $kx = 10^{-5}(x \simeq 2\ pm)$ as shown by the red dot in this figure. The offset creates a static field at the AS port which acts as a local oscillator for the audio frequency gravitational wave sidebands emanating from the IFO. Expanding Eq. 1 to first order for small fluctuations δx around an offset x_0,

$$P_{AS}(x_0 + \delta x) = 4\,g_{cav}^2 P_{BS} k^2 \left(x_0^2 + 2x_0 \delta x \right). \tag{3}$$

We have recovered a linear sensitivity to the audio sidebands with the added advantage that the local oscillator is a) filtered by the coupled cavity pole and b) of exactly the same spatial mode as the GW signal. This equation can be recast in terms of the Relative Intensity Noise at the AS port,

$$RIN_{AS} = \frac{P_{AS}(\omega)}{P_{AS}(\omega = 0)} = 2\frac{\delta x}{x_0}. \tag{4}$$

1.2 AS port power requirements

The amount of power detected at the AS port depends quadratically on the fringe offset. Hence, a reasonable question is, "How large an offset is required to optimize the DARM signal to noise?" In a perfect world with a perfect interferometer, the only noise is the shot noise arising from the DC offset - the term proportional to x_0^2 in Eq. 3 above. The signal to noise ratio is

$$SNR \propto \frac{8\,g_{cav}^2\,P_{BS}\,k^2\,x_0\delta x}{\sqrt{4\,g_{cav}^2 P_{BS} k^2 x_0^2}} = 4g_{cav}\sqrt{P_{BS}}k\delta x. \tag{5}$$

The DARM SNR is proportional to $\sqrt{P_{BS}}$ which explains the increase in laser power for Enhanced LIGO. Counter-intuitively, the signal to noise ratio *does not* depend on the fringe offset for an ideal IFO. Thus we could choose any convenient non-zero offset and be content with the SNR.

However, the dynamic range of the interferometer does place limits on the required light power. Fig. 2 shows the residual length motion for the H1 DARM degree of freedom during
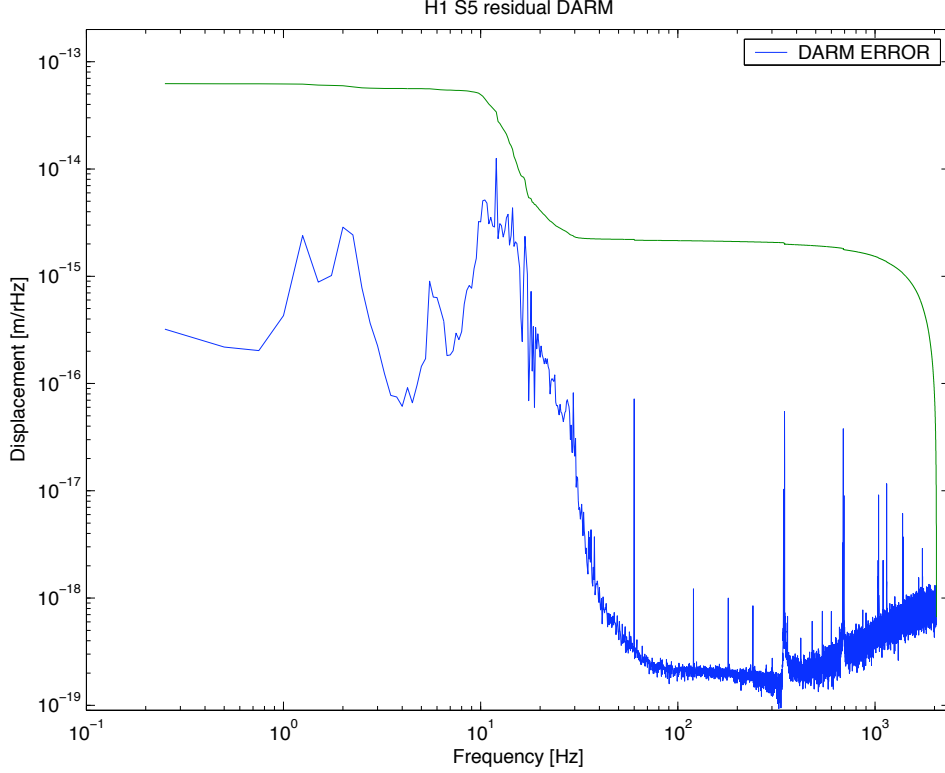
Figure 2: The in-loop residual DARM motion for an H1, S5, science mode lock.

S5 science mode data. The RMS motion of the DARM degree of freedom is approximately 10^{-13} m while the noise floor at 100 Hz is 10^{-19} m. The RMS fluctuations at the AS port should be significantly smaller than the fringe offset so that the DC signal remains linear. If we demand that the DARM RMS fluctuations are 1% of the static power at the AS port, then the minimum RIN is $\sim 10^{-8}$.Thus we must sense at least 1 mW of DARM offset power at the AS port in order to recover S5 shot-noise limited sensitivity. To improve on S5 by a factor of 3 we must sense at least 10 mW.

The upper limit on the sensed DC port power is somewhat more flexible. The DARM readout will have two photodiodes so that we can easily perform out of loop measurements of the DC noise. The 3 mm GTran photodiodes can handle 100 mW of power without damage. Thus 200 mW is the maximum detectable dark port power. To include a safety margin, we are designing for 100 mW total AS port power. Using Eq. 3, 100 mW corresponds to $x_0 \sim 5$ pm. Note that this offset is approximately a factor of 100 larger than the $\leq 10^{-13}$ m residual DARM RMS.

1.3   Output Mode Cleaner

Unfortunately, the LIGO interferometers are not ideal in the DC readout sense since there is significant power at the AS port even with no DARM offset. The light arises from RF sidebands, junk light, and the contrast defect. An Output Mode Cleaner (OMC) is required to filter the AS port light so that only the DARM field is incident on the DC photo-detectors.

The OMC consists of a Fabry-Perot cavity with length, g-factor, and finesse chosen to optimally filter the sidebands and junk light from the desired DARM signal.

The RF readout scheme delivers tens of milliwatts of RF sideband light to the AS port during normal IFO operation to use as a reference field. Although the RF sidebands are likely to be the largest field component at the AS port, they can be distinguished from the DC readout DARM field since they have a known RF frequency shift of 24.5 MHz (61.3 MHz) for the resonant (non-resonant) sidebands. The length of the OMC is chosen such that the RF sidebands contribute the minimum possible power to the output port ($P_{min} \simeq \pi^2/4F^2$).

More difficult to distinguish is carrier "junk light" at the dark port which has no RF offset but is not in the same spatial mode as the DARM field. The junk light is generated by the mode mismatch between the arm cavity fields, imperfect coupling between the recycling cavity and the arms, alignment fluctuations, and the astigmatism introduced by wedged optics. However, the junk light may also be distinguished from DARM light because it does not occupy the DARM spatial mode. If we consider the light at the AS port in the OMC spatial mode basis, the junk light is the Higher Order Mode (HOM) fields. After the OMC length is set by the RF sideband filtering, the cavity mirror radius of curvature is set so that low order HOM do not co-resonate with the OMC carrier mode.

Finally, the arm cavities do not have perfectly matched reflectivities and absorptions, thus generating a contrast defect. Since the contrast defect is (as defined here) the same spatial mode and RF frequency as the DARM field, it cannot be distinguished from DARM motion and presents an irreducible background. A static contrast defect only affects the DARM readout inasmuch as it generates excess shot noise. However, if the contrast defect fluctuates at audio frequencies because of alignment or another dirt effect it can generate excess noise. The intensity fluctuations of the contrast defect place a lower limit on the required DC readout power and DARM offset in addition to the offset described in §1.2.

For a lossy Fabry-Perot cavity, the OMC transmitted power depends on the input power as

$$P_{OMC} = \frac{t_1^2 t_2^2}{(1-\rho r_1 r_2)^2} \frac{P_{AS}}{1 + 4F_{OMC}^2/\pi^2 \sin^2 \phi_{OMC}} \tag{6}$$

$$\equiv g_{OMC} t_2^2 \frac{P_{AS}}{1 + 4F_{OMC}^2/\pi^2 \sin^2 \phi_{OMC}} \tag{7}$$

where we have defined the OMC optical gain $g_{OMC} = t_1^2/(1-\rho r_1 r_2)^2$ as a function of the round trip cavity power loss $L = 1 - \rho^2$. The OMC Finesse is defined similarly, $F_{OMC} = \pi\sqrt{\rho r_1 r_2}/(1-\rho r_1 r_2)$. The OMC length, l, with $\phi_{OMC} = kl$, is set so that the DARM carrier transmission is maximized, $\phi_{OMC}^c = n\pi$ and $P_{OMC}^c = g_{OMC} t_2^2 P_{AS}^c$. The resonant transmission is maximized when $r_2 = r_1\rho \approx r_1$. The RF sidebands and the HOMs are held off resonance where the transmission is minimized, $P_{OMC}^{RF} \approx g_{OMC} t_2^2 \pi^2/4F^2 P_{AS}^{RF}$.

The carrier transmission loss coefficient and the sideband (and HOM) transmission coefficient are shown in Fig. 3 for various assumed cavity losses and coupler reflectivities. The OMC should minimize the carrier loss shown in the dashed lines (ie. maximize the carrier transmission) while also minimizing the sideband transmission shown in the solid lines (ie. maximize the filtering). The colors correspond to round trip losses of 10 ppm, 100 ppm, and 1,000 ppm for blue, green and red respectively. For a sense of scale, 30 ppm is the transmission of an REO high reflector at 6° incident angle. 100 ppm absorption is reasonable for a

cavity of the OMC's design. To keep the carrier loss $\leq 1\%$, the mirror reflectivity is 99.2%, $F_{OMC} = 400$ and the RF and HOM sideband filtering is $P^{RF}_{OMC} \approx 2 \times 10^{-3}$.
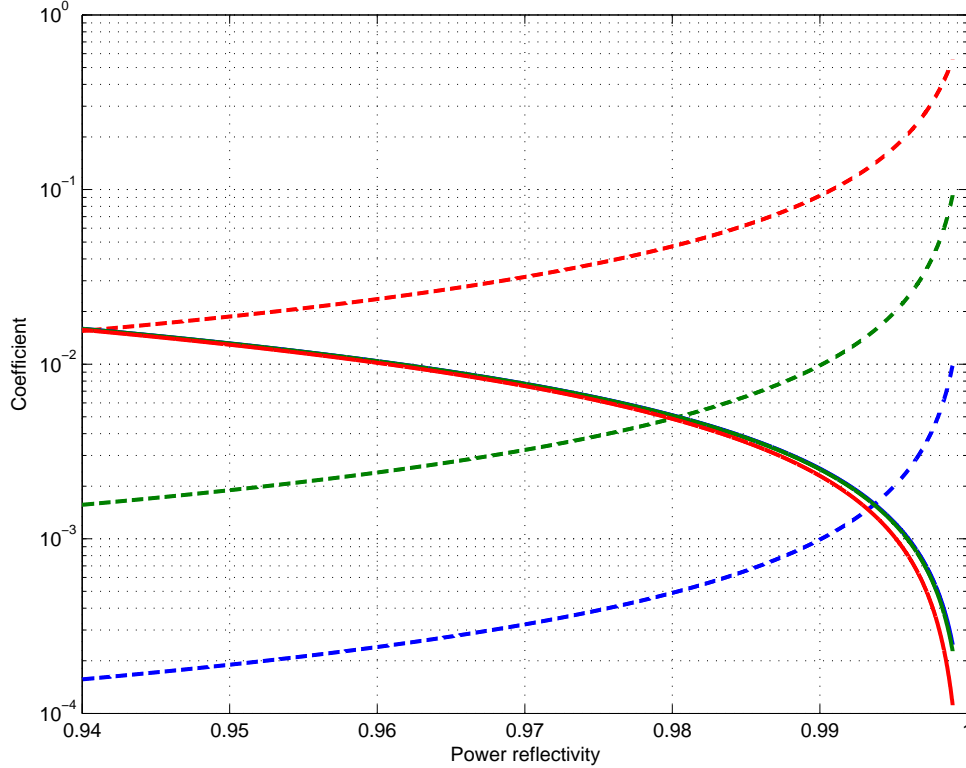

Figure 3: OMC loss (transmission) coefficients for the DARM carrier (RF sidebands) as a function of the coupler reflectivity. The blue, green and red curves are for round trip loss of 10 ppm, 100 ppm, and 1,000 ppm respectively. Dashed lines are the carrier loss coefficient, solid lines are the sideband transmission coefficient.

1.4   OMC g-factor and Guoy phase

Having specified the DARM offset and the OMC finesse, we now specify the OMC length and radius of curvature by examining the detailed mode spectrum. The OMC can be modeled as a two mirror, linear Fabry-Perot cavity of length, L, and mirror radius of curvature, R. Ignoring diffraction from the finite mirror extent, we model the OMC cavity modes as Hermite-Gaussian modes with the (1-D) wave-function

$$\psi_n(r, z) = \sqrt{\frac{1}{q(z)}} \exp\left[-i\frac{kx^2}{2q(z)} - i\left(n + 1/2\right)\phi_G(z)\right] H_n\left(\frac{\sqrt{2}x}{\omega(z)}\right). \tag{8}$$

The term $q(z)$ is the complex Gaussian beam parameter,

$$\frac{1}{q(z)} = \frac{1}{R(z)} - i\frac{\lambda}{\pi\omega(z)^2}, \tag{9}$$

where $R(z)$ and $\omega(z)$ are the radius of curvature and waist size of the Gaussian beam, H_n is the nth Hermite polynomial which describes the transverse profile of the beam, and

$\phi_G(z) = \angle q(z)^{-1}$ is the Guoy phase accumulated relative to a plane wave for a Gaussian beam.

The Guoy phase can be simply related to the Rayleigh range, z_R, and the displacement z as

$$\angle q(z)^{-1} = \arctan z/z_R \tag{10}$$

For a symmetric cavity of length L, the Rayleigh range is

$$z_R = \frac{L}{2}\sqrt{\frac{1+g}{1-g}} \tag{11}$$

where the cavity g-factor is related to the mirror radius and cavity length by $g = 1 - L/R$. After a bit of algebra and trigonometry, we find the cavity Guoy phase as

$$\begin{aligned} \phi_n^{cav} &= (n + 1/2)\left[\arctan(L/2)/z_R - \arctan(-L/2)/z_R\right] \\ &= (n + 1/2)\arccos(g). \tag{12} \end{aligned}$$

Physically, the Guoy phase can be considered the frequency shift relative to the TEM00 mode required to bring a higher order spatial mode into resonance. For instance, for $g = 0.75$, $\phi_1^{cav} = \arccos 0.75 = 0.23\pi$, and the cavity length (or laser frequency) would have to shift upwards by $\sim \pi/4$ (or downwards by $\sim 3\pi/4$) in order to bring the TEM10 mode into resonance.

Since purpose of the OMC is to prevent the transmission of higher order modes to the readout photodiodes, we have chosen a cavity g-factor for which no low order (eg. TEM20 carrier or TEM23 RF) spatial modes resonate near the TEM00 carrier. The optimal g-factor depends on the specific details of the frequency and spatial spectrum of modes at the AS port, such as the L1 spectrum shown in Fig. 4. However, spectra like these depend strongly on the details of the interferometer optics, alignment, and thermal state. Consequently, we designed the OMC using a model in which the power in each higher order mode was proportional to $1/n^2$ and the RF sidebands had their nominal S5 power, $\Gamma = 0.1$.

The spectrum for the H1 OMC using as-built parameters is shown in Fig. 5. In the left panel, the input frequency is swept from -300 MHz to 300 MHz covering two FSRs and reproducing a spectrum qualitatively similar to 4. The right panel shows a zoom in near the resonating carrier showing that contributions from the upper RF, lower RF and carrier signals contribute $\sim 10^{-3}$ of the light transmitted through the OMC (for this model of HOM power). For the H1 OMC, $g = 0.725$ and as a result the 4th order mode carrier mode is nearly resonant the TEM00 mode; $4 \times \phi_G = 0.97\pi$, corresponding to a frequency shift of $f_4 \approx 9$ MHz. Of equal consequence, the 8th and 12th order higher order modes of the lower sideband are also near resonance. Thus the excess intensity noise of the OMC will depend in part on the alignment fluctuations of the carrier and the lower RF sideband.

1.5   OMC topology and length

Having set the OMC finesse and g-factor, we now set the OMC topology and length. The topology is determined by three factors: reduce scattering from the OMC into the IFO, reduce the number of HOM resonances, and maximize the length. The first constraint
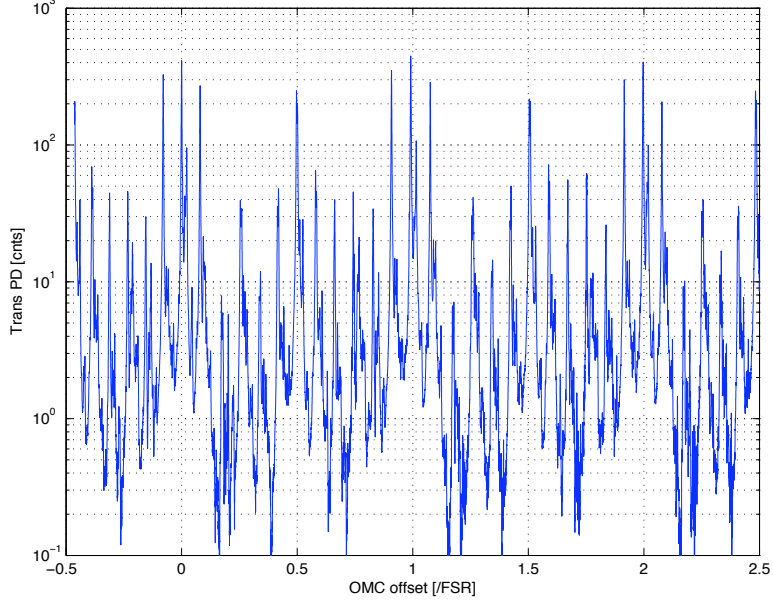
Figure 4: Frequency spectrum of the L1 AS port with a 4 W lock. The highest peaks are the carrier (DARM) TEM00 mode at 0,1, and 2 FSRs and the upper and lower RF sidebands. The peak at 0.5 FSR is the TEM11 mode arising from mode mismatching.
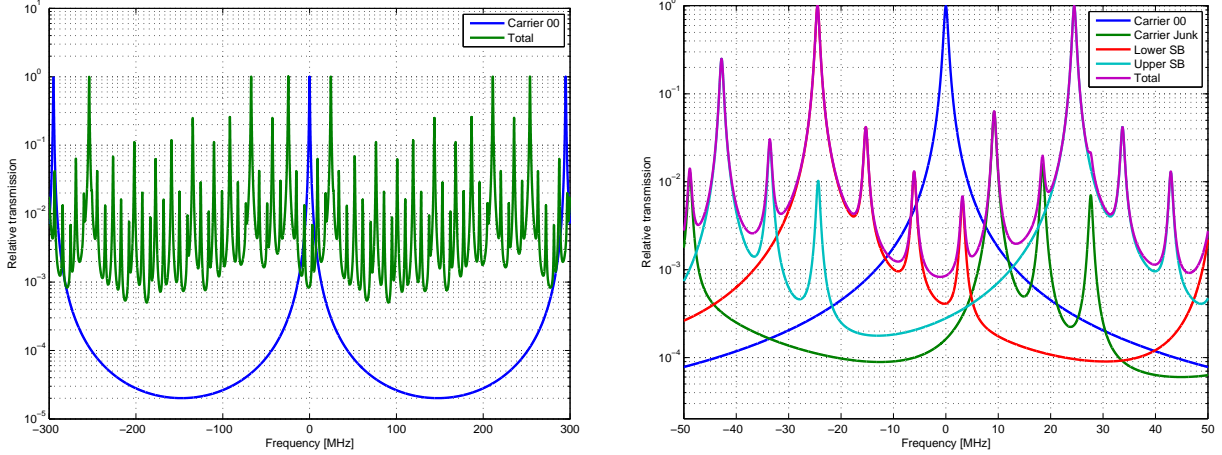

Figure 5: Theoretical transmission spectra for the H1 OMC using the as-build g-factor.

trivially rules out a two-mirror linear Fabry Perot topology. Less trivially, super polished mirrors have a Bidirectional Reflectance Distribution Function (BRDF) that peaks at $0°$ angle of incidence and falls off quadratically until $\approx 5°$, after which it follows a power law distribution. Thus, all the OMC mirrors should have at least $5°$ angle of incidence, particularly since a back reflected beam will see the full OMC cavity gain as it resonates in the counter-propagating mode.

Fig. 6 shows the phase shift in reflection of odd parity TEM spatial modes. In these figures, the laser beam with a TEM10 or TEM01 mode is incident on a mirror from the bottom and is reflected in the $x - z$ plane. For the vertical mode, TEM10, the spatial node lies in the $x - z$ plane and the outgoing mode is identical to the incoming mode upon refection. For the
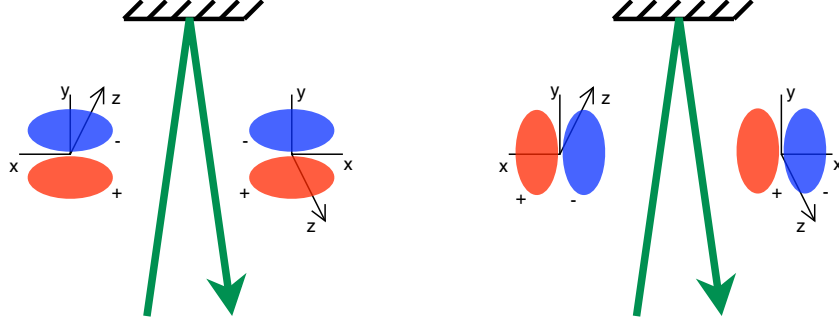
Figure 6: The effect of reflections on the phase of odd-parity spatial modes. The beam is reflected in the x-z plane.

horizontal mode, TEM01, the node lies in the $y - z$ plane and the outgoing mode experiences a π phase shift upon reflection. In other words, for the incoming beam the positive anti-node lies to $+x$ while for the outgoing beam the negative anti-node lies to $+x$, a net change of -1.

This inversion under reflection is true for all odd-parity modes. For a cavity with an odd number of reflections in a given plane, the odd-parity spatial modes in that plane will accumulate an additional π phase shift. This shift is relative to both even-parity modes and to modes in the transverse plane if there are no (or an even number of) transverse reflections. The added phase changes the resonant frequency by π, effectively doubling the number of modes resonating in a given frequency range. The analyses in Fig. 4 and 5 all assume an even number of reflections.

In light of these constraints, we have chosen a four mirror bow-tie cavity with two curved mirrors as shown in schematically in Fig. 7. The "symmetric" form of the bow-tie was chosen to maximize the path length in a fixed area given by the subtrate size which is in turn set by the OMC suspension. The OMC lengths are constrained by the construction to $L = 0.3 - 0.8m$, and the mirror radii of curvature are standard curvatures. For the H1 and L1 OMCs, the g-factor is ~ 0.75, the total cavity length is constrained by the substrate to $L \sim 0.5\ m$, and therefore the mirror radius is $1/(1 - 0.5) = 2\ m$. With ring cavities (including the bow-tie), we often refer to the cavity *perimeter*, $p = 2L \sim 1\ m$, so there is no ambiguity in cavity lengths.
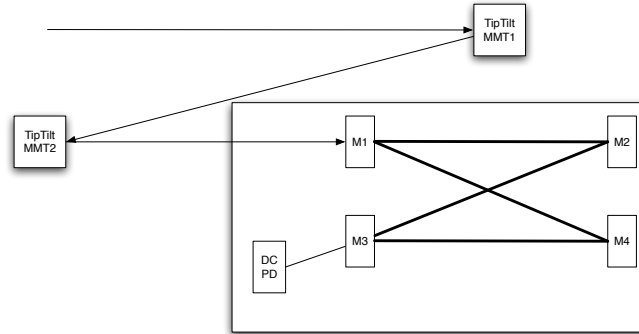

Figure 7: A schematic outline of the OMC topology.

2 Length Control

The output mode cleaner transmitted light should be shot noise limited with 100 mA photocurrent from 200 Hz to 6 kHz. Below 200 Hz, the transmitted light is dominated by the DARM signal and is no longer shot noise limited. In order to meet this noise requirement, the OMC should add 10% of shot noise above 200 Hz and less than 10% of the expected DARM signal below 200 Hz.

2.1 Length noise requirements

For the OMC (and all critically coupled Fabry Perot cavities), the transmitted power, P_T is a function of the OMC length deviation, δx, as

$$P_T(\delta x) = \frac{P_0}{1 + (2\mathcal{F}/pi)^2 \sin^2 k\delta x}. \tag{13}$$

Here P_0 is the light incident on the cavity that we would like to measure, $k = 2\pi/\lambda$ is the wave number, and $\mathcal{F} = \pi/(1 - R)$ is the cavity finesse for a cavity with identical input and output couplers with matched power reflectivity R. For the OMC, the design finesse is $\mathcal{F} \approx 400$. As described in §2.2 the OMC uses feedback control to maximize the transmission by sensing and controlling the cavity length. In this case, $k\delta x \ll 1$ and we expand around $k\delta x = 0$ to get

2.2 Dither locking

2.3 Length range requirements

2.4 PZT actuator

2.5 Thermal actuator

A   L1 Output Mode Cleaner

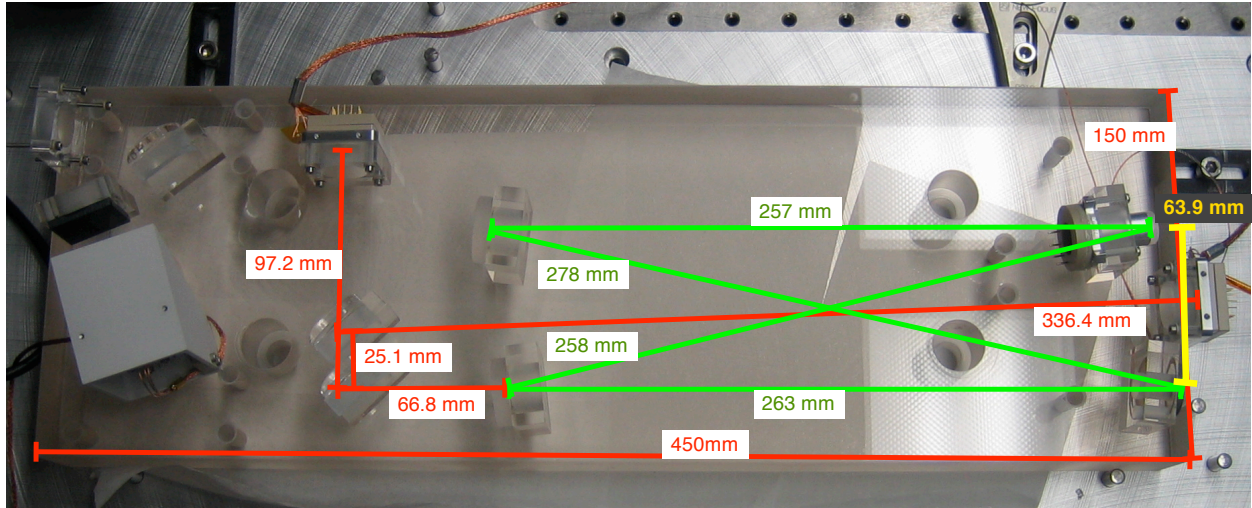| Parameter	Symbol	Design Value	As Built Value
Number of mirrors	N	4	4
Nominal mirror radius	ROC	2 m	1.834 m
Coupler reflectivity	R	8000 ppm	8000 ± 100 ppm
HR Transmission	T_{leak}	0	20 ± 10 ppm
Perimeter	p	1.042 m	1.016 m
Free Spectral Range	FSR	287.7 Mhz	295.2 MHz
Cavity waist	ω	477×10^{-6} m	463×10^{-6} m
Divergence angle	θ_0	0.710 mrad	0.731 mrad
Rayleigh range	Z_R	0.672 m	0.633 m
Mirror Angle of Incidence	AOI	6°	7.2°
HOM frequency shift	f_{HOM}	69.4 MHz	71.8 MHz
Guoy Phase	ϕ_g	42.3°	43.7°
g-factor	g	0.739	0.723
Finesse	$\mathcal{F}$	400	360
Round trip loss	l		
Transmission	T_{OMC}	100%	$\geq 90\%$
DC PZT tuning coefficient	nm/V		1.1 nm/V

Table 1: Livingston OMC parameters.

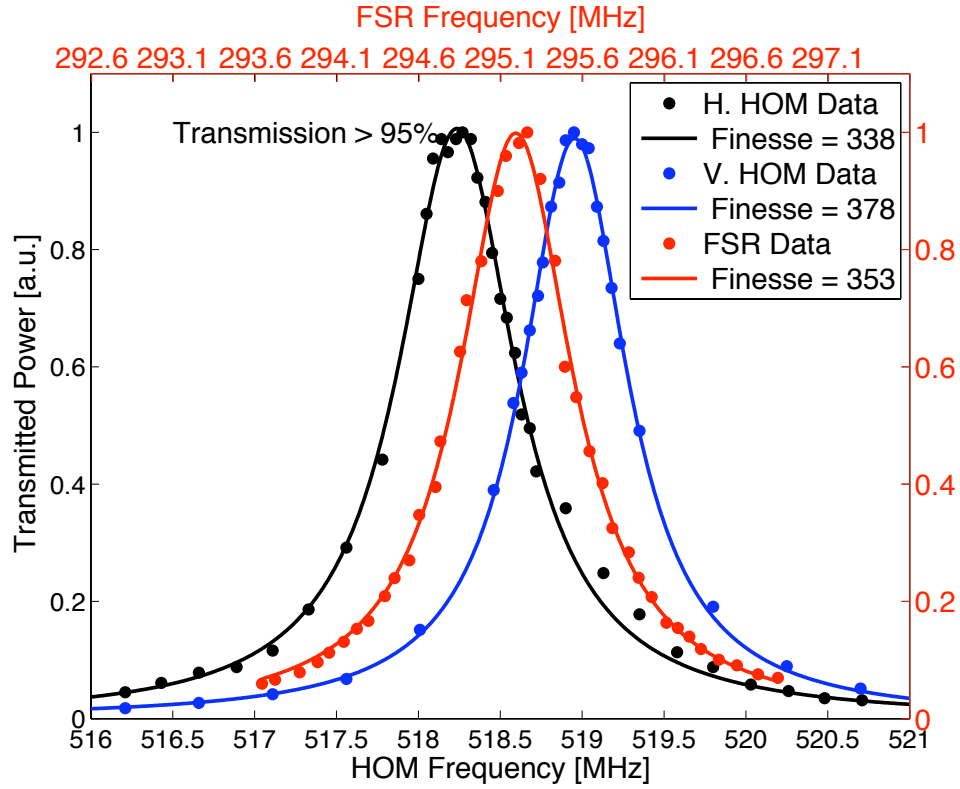Figure 8: L1 OMC lengths. These agree with optical measurements to better than 5%.

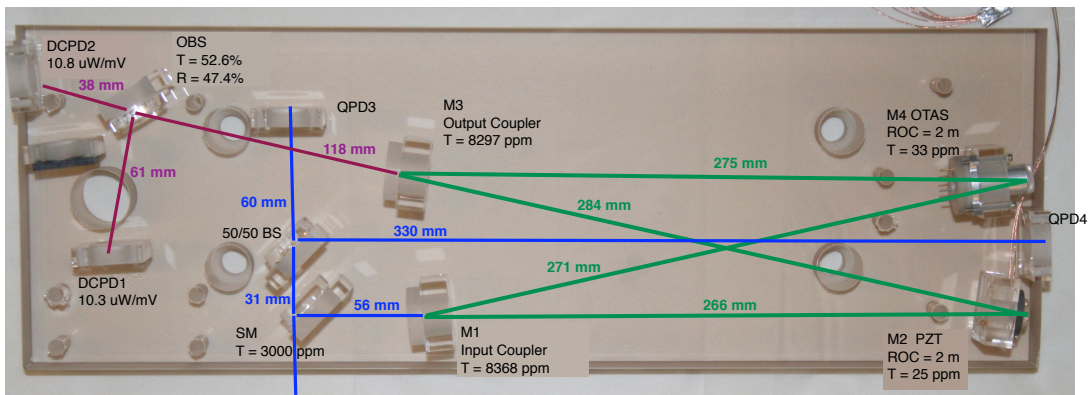Figure 9: Measured L1 OMC FSR and HOM spacing

B   H1 Output Mode Cleaner

Figure 10: H1 OMC lengths. These agree with optical measurements to better than 5%.

| Parameter	Symbol	Design Value	As Built Value
Number of mirrors	N	4	4
Nominal mirror radius	ROC	2 m	1.96 m
Coupler reflectivity	R	8000 ppm	8300 ± 100 ppm
HR Transmission	T_{leak}	0	30 ± 10 ppm
Perimeter	p	1.042 m	1.077 m
Free Spectral Range	FSR	287.7 Mhz	278.3 MHz
Cavity waist	ω	477×10^{-6} m	496×10^{-6} m
Divergence angle	θ_0	0.710 mrad	0.683 mrad
Rayleigh range	Z_R	0.672 m	0.726 m
Mirror Angle of Incidence	AOI	6°	5.5°
HOM frequency shift	f_{HOM}	69.4 MHz	67.2 MHz
Guoy Phase	ϕ_g	42.3°	40.7°
g-factor	g	0.739	0.725
Finesse	$\mathcal{F}$	400	360
Round trip loss	l		
Transmission	T_{OMC}	100%	$\geq 95\%$
DC PZT tuning coefficient	nm/V		0.37

Table 2: Hanford OMC parameters.
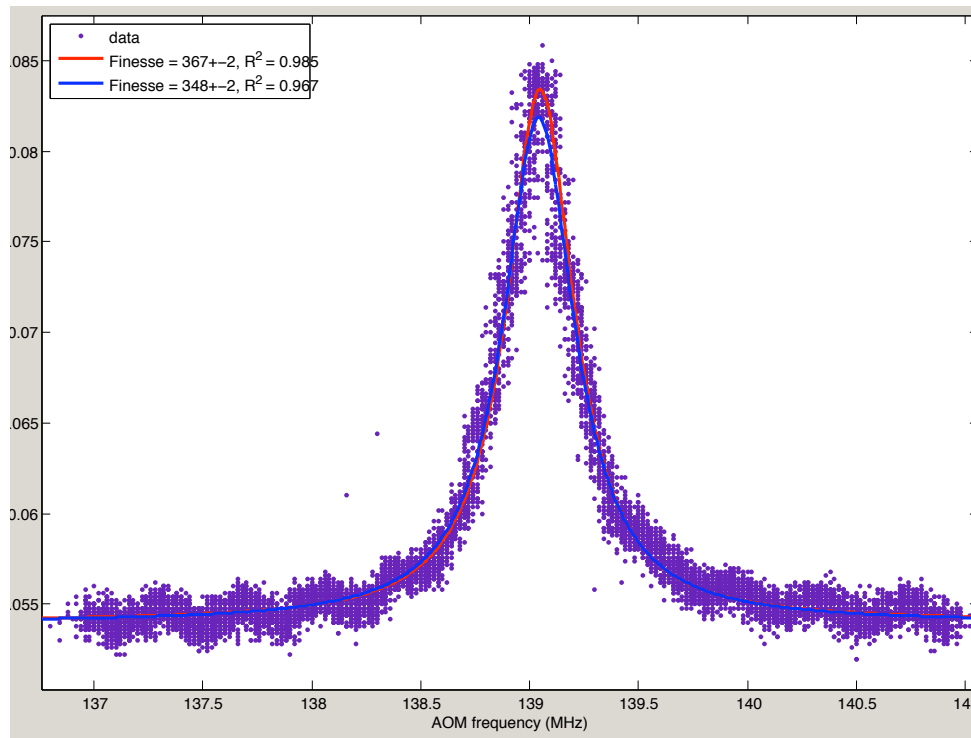
Figure 11: Measured H1 OMC FSR and HOM spacing